How changes in interfacial pH lead to new voltammetric features: the case of the electrochemical oxidation of hydrazine

Antony Cyril Arulrajan, Christophe Renault, Stanley Lai

Chemical Science

ARTICLE

How changes in interfacial pH lead to new voltammetric features: The case of the electrocatalytic oxidation of hydrazine

Received 00th January 20xx,
Accepted 00th January 20xx

DOI: 10.1039/x0xx00000x

www.rsc.org/

Antony Cyril Arulrajan,[a,†] Christophe Renault [a,†] and Stanley C.S. Lai [a,b,*]

The electrochemical oxidation of hydrazine was investigated in strongly and weakly pH buffered solutions to reveal the role of buffer capacity in proton-electron transfer redox reactions. In sufficiently buffered solutions, a single voltammetric feature was observed. However, increasing the hydrazine concentration (or, equivalently, moving to an insufficiently buffered solution) gave rise to a second voltammetric feature. These results are rationalized with a conceptually simple model and finite element simulations. We demonstrate that the new voltammetric feature is caused by a large change in the pH at the electrode surface as the reaction proceeds. Importantly, we show that the occurrence of additional voltammetric features are general for proton-electron transfer reactions in insufficiently buffered solutions, and should not be confused with changes in the reaction mechanism.

Introduction

Proton-electron transfer reactions[1, 2] are (half-)reactions in which both protons and electrons are transferred. Such reactions are ubiquitous in chemical and biological processes. In particular, many redox reactions which are currently being studied involve the transfer of both protons and electrons, in diverse research fields such as energy generation (*e.g.* the oxidation of hydrogen, hydrazine or small organic molecules, or the reduction of oxygen), fuel generation (*e.g.* CO_2 reduction and water splitting reactions) and bioanalytical chemistry (*e.g.* oxidation of neurotransmitters).

In general terms, proton-electron transfer half-reactions occurring at an electrode surface can be described by equation 1

$$\text{Red} \rightleftharpoons \text{Ox} + m\,\text{H}^+ + n\,\text{e}^- \qquad (1)$$

Here, the oxidation reaction releases protons into the electrolyte solution, whereas reduction consumes protons, and the electrode acts as an electron donor or acceptor. Thus, the electrochemical processes can change the pH at the electrode surface in unbuffered or weakly buffered solution, causing it to differ from the pH of the bulk solution. A variety of techniques has been employed to map such (proton) concentration gradients near electrode surfaces and other interfaces.[3-11] For example, fluorescence confocal laser scanning microscopy has been employed to provide three dimensional images of pH gradients at (arrays of) microelectrodes of various types and configurations resulting from the reduction of *p*-benzoquinone, [3] the hydrogen evolution reaction[4-6] and the oxygen reduction reaction,[4] all of which consume protons, causing an increase in the interfacial pH. This capability to visualize surface pH with an optical method has shown promise as a tool to identify faulty electrodes in a microelectrode array,[4] to electrotitrate on a micrometer scale,[6] and for the identification and screening of electrocatalysts.[5, 11] Alternatively, pH gradients near interfaces can be visualized by means of scanning electrochemical miscroscopy (SECM), using either amperometric[8] or voltammetric probes.[9, 10] Thus, while the formation of a pH gradient at an electrode surface due to proton-electron transfer reactions have been well established, how the interfacial pH change in turn impacts on the kinetics of proton-electron transfer reaction has remained somewhat overlooked.[12, 13]

Here, we investigate the interplay between electron transfer kinetics and interfacial pH changes for electrocatalytic proton-electron transfer reactions, using the oxidation of hydrazine (N_2H_4) as a model system. The electrochemistry of hydrazine is of great interest for fuel cell applications, as it is liquid at room temperature (facilitating transport and storage), has a high theoretical energy density, and its oxidation produces carbon-free products.[14, 15] Furthermore, hydrazine (derivates) are used extensively as precursors in the synthesis of pharmaceuticals and agrochemicals. However, residual hydrazine constitutes a key genotoxic impurity, and consequently there is considerable interest for the (electrochemical) detection of hydrazine.[16, 17] Finally, from a fundamental point of view, hydrazine oxidation

[a] *MESA+ Institute for Nanotechnology, University of Twente, P.O. Box 217, 7500 AE Enschede, The Netherlands*
[b] *Current address: Syngenta, Jealott's Hill International Research Centre, Bracknell RG42 6EY, Berkshire, United Kingdom*
† These authors contributed equally
* Corresponding author: E-mail:stanley_chi.lai@syngenta.com; s.c.s.lai@utwente.nl
Electronic Supplementary Information (ESI) available: [details of any supplementary information available should be included here]. See DOI: 10.1039/x0xx00000x

is often employed as a model electrocatalytic system as the onset potential strongly depends on the electrode material and structure, yet quickly reaches mass transport limitations once the onset potential is exceeded. This makes it, for example, a popular choice for a redox probe in nanoparticle collision experiments.[18-22] The overall reaction (in acidic and neutral media) is given by equation 2:

$$N_2H_5^+ \rightarrow N_2 + 5\ H^+ + 4\ e^- \qquad E^0 = -0.33\ V\ vs\ NHE \quad (2)$$

It is generally accepted that the reaction on platinum is initiated by the reversible adsorption of (the deprotonated form of) hydrazine at a vacant surface site, followed by step-wise deprotonation steps that leave the N-N bond intact. There is some debate on rate-determining step, which may depend on the structure of the electrode surface as well as electrolyte composition.[23-25] Regardless of the precise mechanism, voltammetric profiles of hydrazine oxidation typically show a single irreversible voltammetric feature.[25-27]
In this work, we employ hydrazine oxidation as an exemplar electrocatalytic proton-electron transfer reaction involving both adsorption and reaction steps and at both macroscopic (mm-size) and microscopic platinum electrodes in pH-buffered electrolyte solutions. Importantly, we will highlight the importance of buffer concentration in studying proton-electron transfer reactions. Finally, we will demonstrate with a simple fundamental model how the use of insufficiently buffered solutions can cause unexpected voltammetric profiles for proton-electron transfer reactions.

Experimental

Chemicals

Hydrazine (N_2H_4, 35 wt. % in water, Sigma Aldrich), phosphoric acid (H_3PO_4, 85 wt.% in water, Alfa Aesar), sodium dihydrogen phosphate (NaH_2PO_4, > 98%, Sigma Aldrich), sodium hydrogen phosphate (Na_2HPO_4, > 98.5%, Sigma Aldrich), sulfuric acid (H_2SO_4, 99.999%, Sigma Aldrich) were used as received. All solutions were prepared freshly before each experiment with ultra-pure water (Millipore Milli-Q Advantage A10, 18.2 MΩ cm, 2 - 4 ppb total organic content) and deoxygenated by purging with nitrogen for at least 15 minutes.

Electrochemical measurements

Electrochemical measurements were carried out in a conventional three-electrode setup. The working electrode was either polycrystalline Pt disk embedded in a polychlorotrifluoroethylene (PTCFE) shroud (1.6 mm diameter, BASi) or a Pt ultramicroelectrode (UME) encased in glass (10 μm diameter, BASi). The working electrodes were cleaned by mechanical polishing with alumina suspensions of progressively smaller particles size (1.0, 0.3 and 0.05 μm, Buehler), rinsed with copious amounts of ultra-pure water and treated ultrasonically. Finally, the Pt electrode was cycled voltammetrically between the onset of hydrogen evolution and oxygen evolution in 0.1 M H_2SO_4 at 200 mV s^{-1} to ensure a clean surface, as witnessed by a stable voltammogram with well-defined hydrogen underpotential deposition and oxide formation/reduction features. All experiments employed a Pt wire counter electrode and a silver/silver chloride (Ag/AgCl in 3 M NaCl, BASi) reference electrode (E^0 = 0.21 V vs NHE). Voltammetric measurements were performed at room temperature (22 ± 1 °C) using a computer controlled CHI842B potentiostat (CH Instruments). All potentials in this paper are reported against the Ag/AgCl reference electrode employed. The currents are presented as current densities (current normalized by the geometric area of the electrode) for measurements with macroscopic electrodes, and as measured currents (*i.e.* not normalized) for UME measurements.

Finite element method

All simulations were performed using the finite element method (FEM) modeling package Comsol Multiphysics 4.4 running on a personal computer with a 3.4 GHz processor and equipped with 8 GB of RAM. Full details on the simulations are provided in the Supporting Information.

Results and discussion

Figure 1a schematically depicts the various physical and chemical processes involved in the hydrazine oxidation reaction in a buffered solution of neutral and acidic pH. Under these conditions, hydrazine predominantly exist in its protonated form, $N_2H_5^+$ ($pK_{a,hydrazine} \approx 8.2$).[28] Other molecular species in the (bulk) solution are protons (H^+) and a conjugate acid-base pair (HA and A^-). In this study, H_3PO_4 and $H_2PO_4^-$ was used as conjugate acid-base pair for buffer solutions with 1 < pH < 4 (pK_a = 2.2), and $H_2PO_4^-$ and HPO_4^{2-} for pH 6-7 solutions (pK_a = 6.9). Here, the hydrazine oxidation reaction is described by a two step process:

$$N_2H_5^+ + Pt_{site} \rightleftharpoons N_2H_{4,ad} + H^+ \quad (3a)$$
$$N_2H_{4,ad} \rightarrow N_2 + 4\ H^+ + 4\ e^- \quad (3b)$$

Initially, hydrazine in solution is reversibly adsorbed as on a vacant platinum site, releasing one proton in the process (equation 3a). As the electrochemical oxidation reaction is initiated, adsorbed hydrazine is converted to molecular nitrogen, while releasing four electrons and a further four protons (equation 3b). This generates a concentrations gradient, causing a diffusional flux of hydrazine from the bulk solution towards the electrode surface. Meanwhile, the released protons react with the buffer species to establish a new local acid-base equilibrium. This local equilibrium can have concentrations of the participating species which differ from those in the bulk solution, generating a diffusional flux of these species to and from the electrode surface.
A typical cyclic voltammogram (CV) for the oxidation of hydrazine at low concentrations in a phosphate buffer solution (pH 6.9) on a polycrystalline platinum electrode is shown in Figure 1b, along with the corresponding blank CV (*i.e.* without

hydrazine in solution). This CV is in good agreement with those widely reported in literature.[25-27] Under the present working conditions, hydrazine oxidation starts at *ca.* -0.45 V, within the hydrogen underpotential deposition region of the platinum electrode. This corresponds to an overpotential of *ca*. 600 mV, demonstrating that, even on catalytically active materials such as platinum, this reaction is subject to substantial kinetic limitations. Hydrazine oxidation quickly reaches a diffusion-limited peak current at -0.38 V, followed by a broad current plateau.[29] The fact that no reduction peak can be observed further confirms that hydrazine oxidation is an irreversible process (at least in this potential window). The CV for hydrazine oxidation also shows that the characteristics of the blank CV, such as the oxide formation and reduction process, are retained.

As shown in Figure 1c, the pH-dependence of the peak potential and the half-wave potential (*i.e.* the potential at which the current is half of the peak current) for hydrazine oxidation of -72 ± 3 mV / pH unit and -70 ± 3 mV / pH unit, respectively, obtained from CVs for hydrazine oxidation in buffers of varying pH (Supporting Information, SI-1) These (absolute) values are larger than the value expected for a 'trivial' (*i.e.* Nernstian) pH-effect of -59 mV/pH unit, indicating that effects other than the proton concentration contribute to the overall pH-dependence of the reaction In order to gain further insight in the role of possible pH shifts during the hydrazine oxidation reaction, CVs were obtained for solutions with varying hydrazine concentrations, whilst keeping the buffer concentration fixed at 50 mM phosphate (pH 6.9). Figure 2a-i shows the CVs at low hydrazine concentration (0.5, 2 and 5 mM), corresponding to high buffer-to-hydrazine ratios (100, 25 and 10 respectively). It can be seen that under these conditions, the CVs have the typical profile for hydrazine oxidation (*vide supra*). As the hydrazine concentration is increased in this concentration range, the observed currents increase proportionally, ~~and the oxidation peak current shifts towards more positive potentials,~~ as expected for a diffusion-limited irreversible electrochemical reaction.[29] A further increase of the hydrazine concentration to 7 and 10 mM (buffer-to-hydrazine ratios of 7.1 and 5; Figure 2a-ii) gives rise to a second oxidation peak, at approximately 0 – 0.1 V. A closer inspection further reveals that both the magnitude and the position of the first (initial) oxidation peak become nearly independent of the hydrazine concentration. Similar double-peaked voltammetric profiles have been previously been reported for the hydroquinone/*p*-benzoquinone redox couple[13, 30-32] and the hydrogen oxidation/evolution reactions[12] (both of which involves the exchange of two protons and two electrons) in minimally buffered and unbuffered solutions. Various mechanisms have been put forward for this behavior, including changes in interfacial pH,[12, 13] variations in the protonation state of the redox species,[32] differences in basicity of solution species,[30] and changes in the reaction mechanism.[31]

While it is tempting to assign the two oxidation features to a multi-step mechanism, here we will argue that the main cause of the appearance of a second voltammetric feature in the oxidation of hydrazine is the result of changes of the interfacial pH during the reaction. In particular, we will show that the appearance of the second voltammetric feature is caused by a shift in the adsorption equilibrium preceding the electrochemical reaction. To illustrate this concept, we have employed FEM modeling to set up a general model for proton-electron transfer reactions. This model is described in detail in Supporting Information (SI-2). Conceptually, the model is fairly simple, and consists of the four elements outlined in Figure 1a, namely diffusional mass transport of species to and from the electrode surface, a solution-phase acid-base equilibrium, a hydrazine adsorption equilibrium at the electrode surface and the electrochemical reaction of adsorbed hydrazine. Mass transport and the acid-base equilibrium are described by Fick's diffusion laws and the Henderson-Hasselbach equation, respectively. The adsorption equilibrium is described by a Langmuir isotherm:

$$K_{ads} = \frac{[N_2H_4][H^+]}{[N_2H_5^+][Pt]} \quad (4)$$

, where $[N_2H_{4,ad}]$ and [Pt] are surface concentrations (in mol cm^{-2}), while $[N_2H_5]$ and $[H^+]$ are volume concentrations (mol cm^{-3}). Both the acid-base and adsorption equilibria are considered to be fast (at equilibrium) compared to the diffusion of species and the electron transfer kinetics.
Finally, the electron transfer is described by a Butler-Volmer-like relationship for an irreversible reaction (equation 5):

$$j = nFDCk^0 \exp[(1-\alpha)\frac{n_{app}F}{RT}(E_{app} - E^0)] \quad (5)$$

, where *F*, *R* and *T* are defined previously, E^0 is the formal potential for the reaction of $N_2H_{4,ads}$ (equation 3b), *j* is the current density, *C* is the (pH-dependent) surface concentration of adsorbed hydrazine, E_{app} is the applied potential, *D* is the diffusion coefficient of hydrazine, k^0 is the heterogeneous electron transfer rate constant, α is the transfer coefficient, and n_{app} is the number of electrons exchanged in the rate determining step. It is important to note that we do not assign a specific molecular mechanism to the hydrazine oxidation reaction, other than the presence of a pre-adsorption step. While we recognize that this may be simplified interpretation of the hydrazine oxidation reaction, we will show below that the main concentration dependency of the voltammetric profiles are well captured by this simple model. Furthermore, by not including specific mechanisms for the electrode reaction, we believe insights from this model can be generalized to other proton-electron transfer reactions involving a pre-reaction adsorption step.
The key element of this model is that changes in surface pH are reflected in changes of the position of adsorption equilibrium in equation 3a, thereby changing the activity of the

Commenté [CR1]: Ep is independent of C(N2H5) for an irreversible electron transfer.

reduced species in the electrochemical step (equation 3b). Using this model, we have simulated CVs for hydrazine oxidation, shown in Figure 2b. Comparing the simulated CVs with the experimentally obtained CVs, it is clear that the main features of the CVs are extremely well reproduced. For example, both the magnitude and the position of the first oxidation peak at different hydrazine concentrations are in good agreement. Importantly, the model predicts the appearance of a second voltammetric feature when the hydrazine concentration exceeds a certain threshold. Furthermore, both the position and the absolute magnitude of the second feature are reproduced reasonably by the simulations (although less well than that of the first feature), demonstrating that the occurrence of a second peak can be explained through the simple kinetic model employed here.

So how does the interfacial pH affect the voltammetric profile, and what role does the buffer capacity play? In order to answer these questions, one needs to take a closer look at the evolution of the interfacial pH during a voltammetric sweep. Figure 3a shows the interfacial pH as a function of applied potential for the case of a high buffer-to-hydrazine ratio, corresponding to the simulated CVs of 0.5 mM in 50 mM phosphate buffer in Figure 2b-i. In this case the pH starts to decrease at the onset of hydrazine oxidation (ca. -0.45 V). The pH continues dropping as long as the hydrazine oxidation takes place, as the reaction continuously releases protons into the solution, until a quasi-steady state is reached. However, the decrease in pH is limited to only *ca.* 0.1 pH unit, indicating that in this case the buffer manages to maintain the solution pH as expected. Thus, the 'bulk' concentration of the reacting species in the electrochemical step ($N_2H_{4,ad}$) does not change, and a 'regular' CV is obtained.

At low buffer-to-hydrazine ratio, on the other hand, such as the case for 10 mM hydrazine in 50 mM pH buffer (*c.f.* Figure 2b-ii), the pH change is much more severe, dropping from the bulk pH of 7.1 to a pH of *ca.* 2.5 at the ~~most driving potential~~largest driving force (Figure 3b). Not surprisingly, this value agrees reasonably with the value which obtained with a crude calculation based on the reaction stoichiometry: 10 mM hydrazine releases 50 mM protons at the surface. As the buffer contains 25 mM of the basic component, half of the released protons are neutralized by the buffer, leaving a 25 mM concentration of protons (pH 1.6). An implicit assumption in this calculation is that all species (hydrazine, protons and buffer components) have equal diffusivities. As the diffusion of protons is significantly higher than the other species, the surface excess of protons will be diminished, resulting in a somewhat higher pH than the approximate calculation. An important consequence of the large pH change is that the position of the adsorption equilibrium changes, as the concentrations during the reaction, and thus the concentration of the reacting adsorbed species, also changes during the reaction. Initially, as long as the pH remains approximately constant, the CV follows the well-known profile as in the well-buffered case. However, as the driving force of the reaction is increased, the buffer becomes unable to maintain the pH and the pH drops sharply. This, in turn, causes a drop in the concentration of the adsorbed reactant species (N_2H_4), giving rise to the first oxidation peak in the voltammogram. At this point, as the potential is further increased, the pH continues to drop, and the resulting voltammogram is a complex interplay between the adsorption equilibrium, changes in equilibrium potential and electrochemical kinetics. Finally, the pH somewhat stabilizes, and application of the potential sweep can again be described using simple electrochemical theory, albeit with a lower concentration of the reactant adsorbed hydrazine., eventually leading to the second oxidation feature. In both cases, the region in which the local pH differs from the bulk pH (*i.e.* proton diffusion layer thickness) can extend up to *ca*. 400 µm into the bulk solution at the highest driving potential (see insets). Thus, conceptually, one can understand the complex voltammetric profile in insufficiently buffered solutions as follows: it essentially comprises two separate voltammetric measurements at different conditions, one at the initial pH of the solution (here, pH 7.1), and one at the surface pH at the end of the voltammetric sweep (here, pH 2.5). The overall voltammetric profile is then approximately the sum of the two separate profiles. Importantly, our findings show that complex voltammetric profile can be fully explained without the need to consider a specific (change in) mechanism for the hydrazine oxidation reaction.

This phenomenon is not only manifested in measurements on macroscopic electrodes, where it could be argued that slow diffusional mass transport rates allow the buildup of protons at the electrode surface, but also at high mass transport rates. This is evident from voltammetric profiles recorded at an UME, as shown in Figure 4a. At low hydrazine concentrations (0.5 mM and 2 mM), the voltammograms are sigmoidal in shape, typical for a (reasonable) facile reaction at a microelectrode. The onset potentials are similar to those observed on macroscopic electrodes, and at potentials above ~ - 0.2 V a clear, well-defined diffusion limited current plateau is observed. Using the equation for the diffusion limited current at a (disc) UME (i_{lim} = 4*nFDCr*, where *D* is the diffusion constant, *r* is the radius of the UME, and *n*, *F* and *C* are as defined previously), a diffusion constant of 1.0×10^{-5} cm^2 s^{-1} can be calculated for hydrazine. This value lies within the reported range for hydrazine,[19, 27, 33, 34] and is typical for small molecules in an aqueous solution. As the hydrazine concentration is increased, the voltammetric profiles start to deviate from the sigmoidal behavior observed at low hydrazine concentrations, eventually giving rise to a second plateau at higher potentials. Previously, the occurrence of a second plateau in the voltammetric profile for hydrazine oxidation at UMEs have typically been attributed to multiple steps in the hydrazine oxidation process, *e.g.* with the first plateau corresponding to the formation of an intermediate species.[22, 35] In this case, one would expect that the ratio of two plateau current would not only be constant, but also correspond to an integer number of electrons for both steps, which is not the case. Additionally, one should take care to select sufficiently wide potential windows for performing voltammetric measurements and ensure a stable steady state current is

reached in with a (relatively) low concentration of buffer species, in order to not make (potentially) erroneous conclusions based on what seems to be diffusion limited current plateau.[18, 20] We believe a key diagnostic is that the final plateau current should scale linearly with the hydrazine concentration such as in Figure 4a, indicating that the overall reaction stoichiometry remains the same.

Using the model outlined above (with minor adjustments to account for the more complex geometry of a UME measurement), the main trends of the transition from a single voltammetric wave to a signal with multiple plateaus as the hydrazine concentration is increased is well reproduced, both in the position and the magnitude of the voltammetric waves (Figure 4b). This clearly illustrates that the appearance of the second plateau is the manifestation of a change in interfacial pH, equivalent to the second oxidation peak at a macroscopic electrode. Furthermore, our results emphasize the importance of selecting sufficiently wide potential windows for performing voltammetric measurements in insufficiently buffered solutions.

Conclusions

In this contribution, we have highlighted the importance of interfacial pH changes during proton-electron transfer reactions using the case of hydrazine oxidation. We show that an additional oxidation feature can appear in a voltammetric measurements at low buffer-to-hydrazine ratios, such as a second peak on macroscopic electrodes or a second current plateau for UMEs. While it is tempting to interpret the occurrence of new voltammetric features as changes in the reaction mechanism, we demonstrate that the main cause is the result of a more trivial consideration. By using a simple model and FEM simulations, we unambiguously demonstrate that the main cause of the appearance of an additional voltammetric feature is the significant pH change at the electrode surface if the buffer capacity is insufficient, due to the protons released by the electrochemical oxidation of hydrazine, causing a progressive shift the adsorption equilibrium of the electrochemically active species.

Importantly, as our model only considers a simplified reaction mechanism, without the need to take the role of the electrode material into account, the effect of interfacial pH changes highlighted herein can be generalized to proton-electron transfer reactions which contain a pH dependent pre-adsorption step, and in which a significant amount of protons (relative to the buffer capacity) are released or consumed. It emphasizes the need to reflect on the buffer capacity of the solution that is employed in a given experiment. This is particularly important in the case of ready-made 'standard' buffers (such as *e.g.* phosphate buffered saline, which only has 10 mM buffer capacity), as one might not consider the buffering capability of the medium, but rather implicitly assumes it is sufficient. Finally, we advocate caution in interpreting additional voltammetric features in buffered electrode solutions as insights in a reaction mechanism, as we show that the main cause of the occurrence of an additional voltammetric feature can be simply related to interfacial pH changes.

Acknowledgements

The authors acknowledge partial financial support from the European Research Council (ERC) under project number 278801. We wish to thank Prof. Serge Lemay (University of Twente) for general support and Dr. Chang-Hui Chen (University of Warwick) for fruitful discussions.

Notes and references

1. D. R. Weinberg, C. J. Gagliardi, J. F. Hull, C. F. Murphy, C. A. Kent, B. C. Westlake, A. Paul, D. H. Ess, D. G. McCafferty and T. J. Meyer, *Chem. Rev.*, 2012, **112**, 4016-4093.
2. M. T. M. Koper, *Chem. Sci.*, 2013, **4**, 2710-2723.
3. S. Cannan, I. Douglas Macklam and P. R. Unwin, *Electrochem. Commun.*, 2002, **4**, 886-892.
4. N. C. Rudd, S. Cannan, E. Bitziou, I. Ciani, A. L. Whitworth and P. R. Unwin, *Anal. Chem.*, 2005, **77**, 6205-6217.
5. A. J. Leenheer and H. A. Atwater, *J. Electrochem. Soc.*, 2012, **159**, H752-H757.
6. S. Fiedler, R. Hagedorn, T. Schnelle, E. Richter, B. Wagner and G. Fuhr, *Anal. Chem.*, 1995, **67**, 820-828.
7. H. Hotta, K. Tatsuno, Y. Hattori, T. Hashimoto, M. Uehara and K.-i. Tsunoda, *Electrochem. Commun.*, 2008, **10**, 1351-1354.
8. Y.-F. Yang and G. Denuault, *J. Chem. Soc., Faraday Trans.*, 1996, **92**, 3791-3798.
9. B. R. Horrocks, M. V. Mirkin, D. T. Pierce, A. J. Bard, G. Nagy and K. Toth, *Anal. Chem.*, 1993, **65**, 1213-1224.
10. M. Etienne, P. Dierkes, T. Erichsen, W. Schuhmann and I. Fritsch, *Electroanalysis*, 2007, **19**, 318-323.
11. E. Reddington, A. Sapienza, B. Gurau, R. Viswanathan, S. Sarangapani, E. S. Smotkin and T. E. Mallouk, *Science*, 1998, **280**, 1735-1737.
12. I. Katsounaros, J. C. Meier, S. O. Klemm, A. A. Topalov, P. U. Biedermann, M. Auinger and K. J. J. Mayrhofer, *Electrochem. Commun.*, 2011, **13**, 634-637.
13. J. Wang, H. Wang, S. Guo, X. Jia, Y. Zhong, Y. Han, M. Lin, S. Wang, F. Zhao, J. Fu and J. Zhao, *J. Electrochem. Soc.*, 2014, **161**, H443-H446.
14. A. Serov and C. Kwak, *Applied Catalysis B: Environmental*, 2010, **98**, 1-9.
15. D. A. Finkelstein, R. Imbeault, S. Garbarino, L. Roué and D. Guay, *J. Phys. Chem. C*, 2016, **120**, 4717-4738.
16. D. Q. Liu, M. Sun and A. S. Kord, *J. Pharm. Biomed. Anal.*, 2010, **51**, 999-1014.
17. R. B. Channon, J. C. Newland, A. W. T. Bristow, A. D. Ray and J. V. Macpherson, *Electroanalysis*, 2013, **25**, 2613-2619.
18. X. Xiao, F.-R. F. Fan, J. Zhou and A. J. Bard, *J. Am. Chem. Soc.*, 2008, **130**, 16669-16677.
19. S. E. F. Kleijn, S. C. S. Lai, T. S. Miller, A. I. Yanson, M. T. M. Koper and P. R. Unwin, *J. Am. Chem. Soc.*, 2012, **134**, 18558-18561.

20. S. J. Percival and B. Zhang, *J. Phys. Chem. C*, 2016, **120**, 20536-20546.
21. D. A. Robinson, J. J. Yoo, A. D. Castañeda, B. Gu, R. Dasari, R. M. Crooks and K. J. Stevenson, *ACS Nano*, 2015, **9**, 7583-7595.
22. A. R. Jung, S. Lee, J. W. Joo, C. Shin, H. Bae, S. G. Moon and S. J. Kwon, *J. Am. Chem. Soc.*, 2015, **137**, 1762-1765.
23. V. Rosca and M. T. M. Koper, *Electrochim. Acta*, 2008, **53**, 5199-5205.
24. B. Álvarez-Ruiz, R. Gómez, J. M. Orts and J. M. Feliu, *J. Electrochem. Soc.*, 2002, **149**, D35-D45.
25. J. A. Harrison and Z. A. Khan, *J. Electroanal. Chem.*, 1970, **28**, 131-138.
26. M. D. García, M. L. Marcos and J. G. Velasco, *Electroanalysis*, 1996, **8**, 267-273.
27. C.-H. Chen, L. Jacobse, K. McKelvey, S. C. S. Lai, M. T. M. Koper and P. R. Unwin, *Anal. Chem.*, 2015, **87**, 5782-5789.
28. *CRC Handbook of Chemistry and Physics*, 1982.
29. A. J. Bard and L. R. Faulkner, *Electrochemical Methods - Fundamentals and Applications*, Wiley, New York, USA, 2000.
30. M. Rafiee and D. Nematollahi, *Electroanalysis*, 2007, **19**, 1382-1386.
31. Y.-B. Shim and S.-M. Park, *J. Electroanal. Chem.*, 1997, **425**, 201-207.
32. M. Quan, D. Sanchez, M. F. Wasylkiw and D. K. Smith, *J. Am. Chem. Soc.*, 2007, **129**, 12847-12856.
33. S. Karp and L. Meites, *J. Am. Chem. Soc.*, 1962, **84**, 906-912.
34. P. V. Dudin, P. R. Unwin and J. V. Macpherson, *Phys. Chem. Chem. Phys.*, 2011, **13**, 17146-17152.
35. Q. Chen, H. S. Wiedenroth, S. R. German and H. S. White, *J. Am. Chem. Soc.*, 2015, **137**, 12064-12069.

1

Chemical Science

ARTICLE

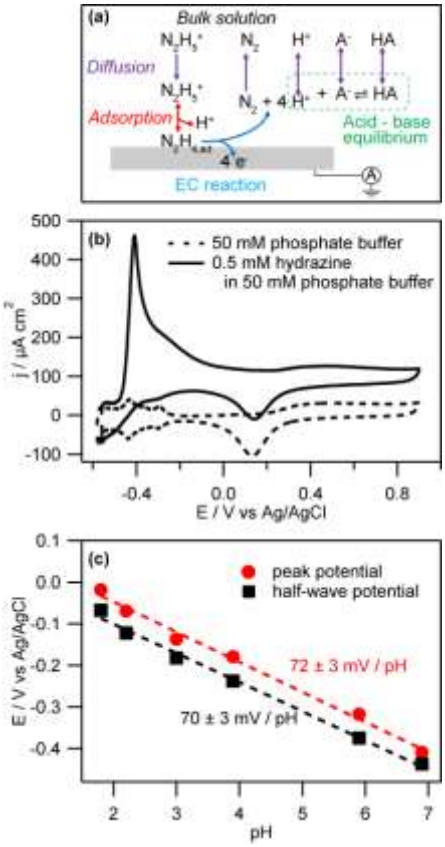

Figure 1: (a) Schematic representation of the hydrazine oxidation reaction in a buffered medium. (b) Cyclic voltammograms of a macroscopic polycrystalline platinum electrode in a 50 mM phosphate buffer (pH 6.9) in the absence (dashed line) and presence (solid line) of 0.5 mM hydrazine. First voltammetric cycle, scan rate 20 mV s-1. (c) Variation of peak potential and half-wave potential as a function of pH, measured in 0.5 mM hydrazine in 50 mM phosphate buffer solutions.

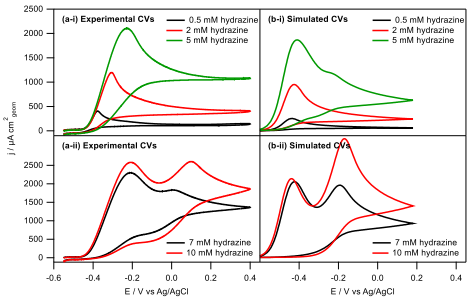

Figure 2: (a) Experimental and (b) simulated cyclic voltammograms for the electrocatalytic oxidation of varying concentrations of hydrazine in a 50 mM phosphate buffer solutions (pH 6.9). First voltammetric cycles, scan rate 20 mV s^{-1}.

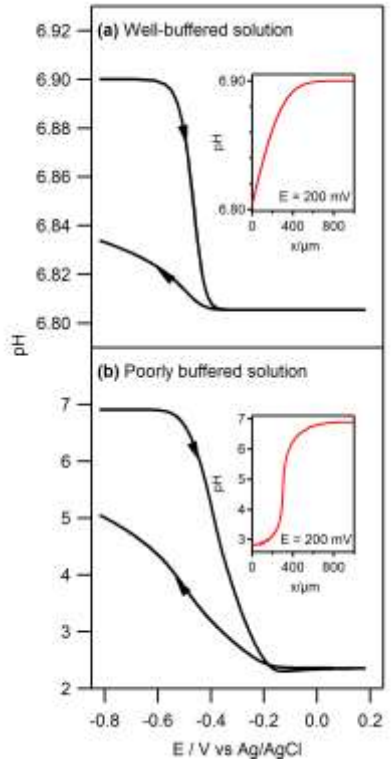

Figure 3: Simulated development of surface pH (left axis) and applied overpotential (right axis) during a voltammetric cycle for hydrazine oxidation in a (a) well-buffered (0.5 mM hydrazine in 50 mM phosphate buffer) and (b) poorly buffered solution (10 mM hydrazine in 50 mM phosphate buffer). The arrows indicate the sweep direction. Insets show the pH profile as a function of distance to the electrode at 200 mV.

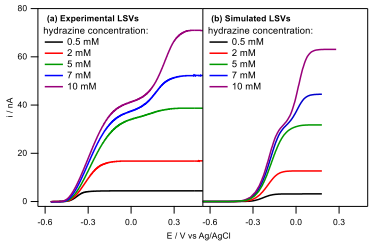

Figure 4 a) Experimental and b) simulated linear sweep voltammograms (LSVs) for the electrocatalytic oxidation of various concentrations of hydrazine in a 50 mM phosphate buffer solution (pH 6.9) on a platinum ultramicroelectrode (r = 5 μm). First voltammetric cycle, scan rate 20 mV s^{-1}.